

Study within the Mining Effects Knowledge Program (KEM-39) on the cyclic storage of gases in the Netherlands

WP4: Set-up of the Numerical Model

Authors:

Eng. Isotton Giovanni¹
Prof. Janna Carlo¹
Prof. Teatini Pietro¹
Prof. Deangeli Chiara²
Prof. Rocca Vera²
Prof. Verga Francesca²
Prof. Collettini Cristiano³

Affiliations:

¹M3E srl
²Politecnico di Torino
³Università la Sapienza

Document type: Technical report

Date: December 2022

INDEX

Introduction.....	3
1 Configuration of the Geomechanical Model.....	4
1.1 Geometry.....	4
1.2 FE Mesh.....	7
1.3 IE Mesh.....	7
1.4 Reference test case set-up.....	8
2 External Forces.....	11
3 Geochemical Effects.....	12
4 Numerical Formulation for Fault Modeling.....	12
4.1 Validation.....	14
5 Final remarks.....	17
References.....	18

Introduction

The WP4 is responsible for the set-up of the numerical model to be used for the analysis of the CO₂, N₂ and H₂ storage scenarios in the next WP. The numerical model, sketched in Figure 1, is the combination between the reservoir model, developed in WP3 [8], and the geomechanical model. These two models are coupled together in the so-called one-way coupling approach: the pore-pressure change computed with the reservoir model are used as external forces in the geomechanical model. The numerical model set-up is performed following two main guidelines agreed with the MEA supervisor:

- it should be as similar as possible to that developed in the KEM-01 project [2,3,4] to facilitate comparisons between CO₂, N₂ and H₂ storage and UGS;
- it must take into account the geochemical effects on rock and fault mechanical parameters according to the results of WP1 [6] and WP2 [7];

The report is subdivided in 5 main sections: (1) configuration of the geomechanical model and definition of the reference test case; (2) definition of the external forces; (3) definition of the geochemical effects to introduce into the model; (4) validation of the numerical formulation used for the fault modelling and (5) final remarks.

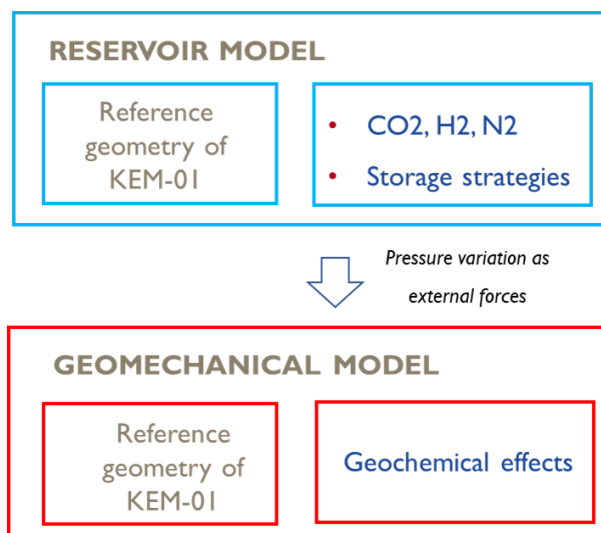


Figure 1: Sketch of the numerical model: reservoir model plus geomechanical model.

I Configuration of the Geomechanical Model

In agreement with the MEA advisor and the representative of the KEM panel, the configuration of the geomechanical model is exactly the same as the one used in KEM-01 [2,3,4]. In the following sections details are provided regarding the geometry, the Finite Element (FE) mesh, the Interface Element (IE) mesh used for the fault modelling and the settings used to define the reference test case.

I.1 Geometry

The plan view of the model is shown in Figure 2. The reservoir, located at the barycentre of the model, is subdivided by fault F3 into two square blocks, 2×2 km wide. Other four faults, namely F1, F2, F4 and F5 bound the reservoir in the four directions West, East, North and South, respectively. The global domain is a square 30 km wide to remove the effect of the boundary conditions on the solution in the area of interest.

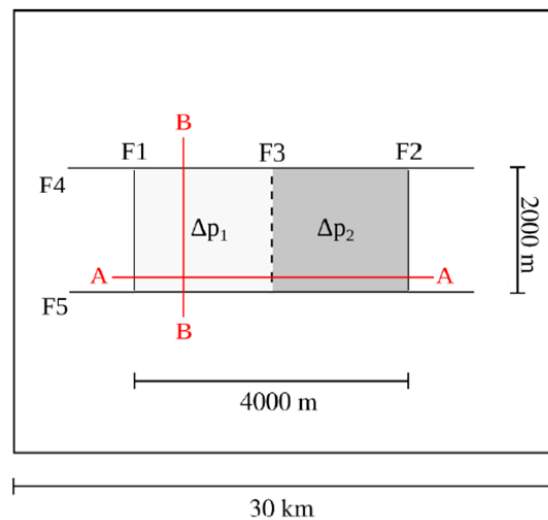


Figure 2: Plan view of the model.

Two vertical cross sections through the reservoir are shown in Figure 3. Faults F1 and F2 have a dip angle equal to 100° and 80° , respectively, while F4 and F5 are vertical (dip angle equal to 90°). The dip angle of fault F3 can vary between 90° (see reference test case in [4]) and 65° (see final combinations in [4]). The faults extend from depth 3km and terminate within the caprock at depth 1.6km.

The thickness of the reservoir is 200m while its top is located at a depth of 2km¹. The top of the domain is located at the elevation 0 m and the model is 5km-thick.

The block 2 of the reservoir can move in the vertical direction with an offset of 100 m (see final combinations in [4]). Along the direction orthogonal to the main F1, F2, and F3 faults (i.e., along the B-B direction of Figure 3), the elevation of the reservoir and caprock formations remain constant.

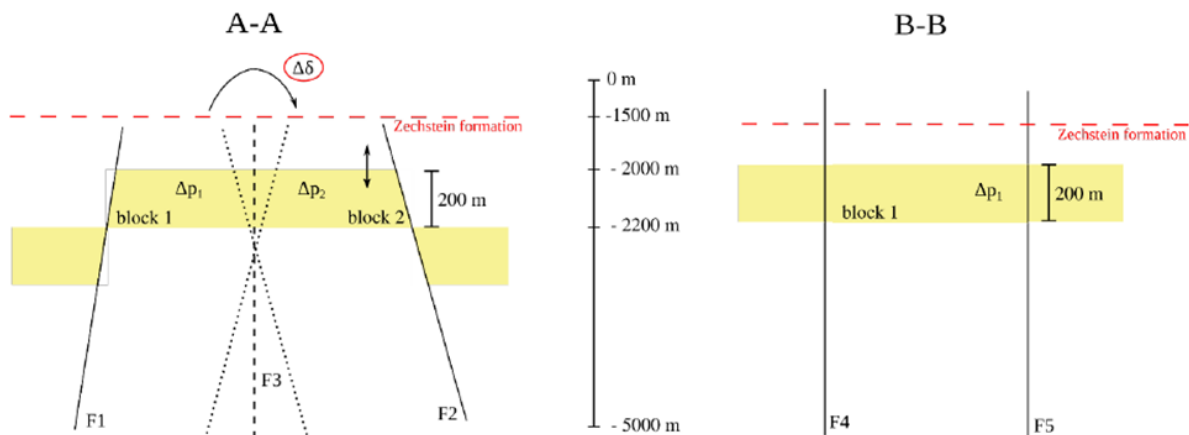


Figure 3: Vertical cross section of the model along the trace A-A and B-B shown in Figure 2.

The selection of a reservoir at a depth smaller (2000 m) than actual values (2500 - 3000 m) is a conservative assumption in terms of fault reactivation, at least for the typical geologic setting of the Rotliegend reservoirs. Observing that a larger depth usually implies a larger overburden load and, consequently, effective stress and a stiffer reservoir formation, it can be concluded that:

- 1) on vertical faults (dip angle = 90°), higher effective stress is stabilizing. In fact, it increases the initial normal effective stress and thus the shear stress limit τ_L for failure condition;
- 2) the same concept holds also for sub-vertical faults, i.e., faults characterized by a gentle slope at typically occurred in the Rotliegend formation;
- 3) a higher stiffness of the field formation decreases the compaction and contraction of the depleted reservoir, thus reducing the development of shear stress and keeping higher the normal stress acting on the fault, respectively. Therefore, as it has been observed in KEM-01 project, it results in a smaller critical index χ for a same pressure change acting within the reservoir blocks.

Concluding, keeping a same history of the pressure change, a comparable or lower values of the parameter χ are expected for faults bounding deeper reservoirs.

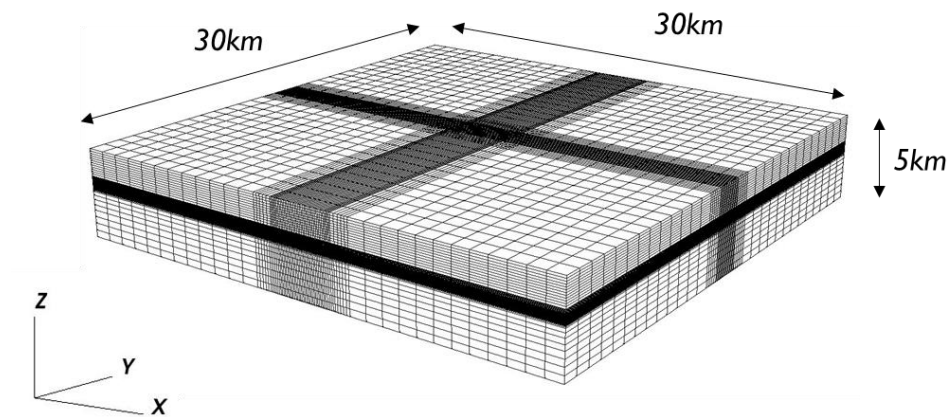


Figure 4: Axonometric view of the 3D-FE mesh.

1.2 FE Mesh

The 3D-FE mesh is developed by using 8-noded hexahedral elements. An axonometric view of the 3D-FE grid used in the geomechanical model is shown in Figure 4. The mesh consists of 271,010 nodes and 252,784 FE elements. The discretization in the XY plane is the same as that used in KEM-01 [3], while, vertically, the model has been slightly refined at the top and bottom of the reservoir. This refinement will be explained in section 2.

1.3 IE Mesh

In the model, the structural discontinuities defined by the faults have been represented by inserting within the FE-mesh so-called Interface Elements (IEs). The IEs, by doubling the nodes lying on the fault surface (Figure 5), allow the simulation of the possible reactivation of the discontinuity if the shear stress τ reaches the critical value defined through a Mohr-Coulomb criterion:

$$\tau_L = c + \sigma_n \tan(\varphi)$$

where τ_L is the maximum shear stress with a normal effective stress σ_n , cohesion c and static friction angle φ . Details regarding the numerical formulation are provided in sections 2.

A total of 6,314 IEs has been used to discretize the 5 faults. Figure 6 shows an axonometric view of the IE-mesh.

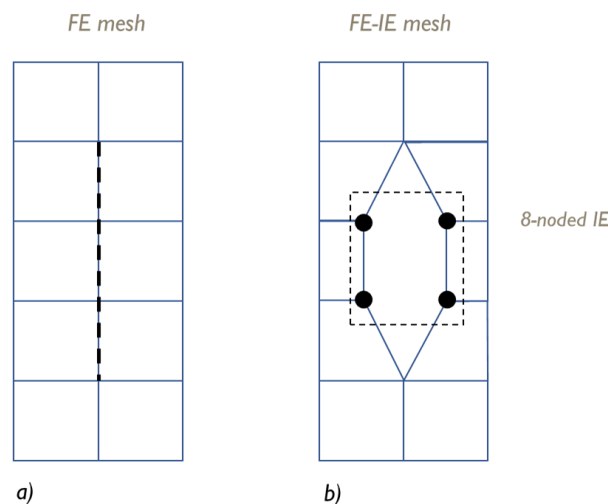


Figure 5: Plan view of: (a) continuous FE grid, the fault line is highlighted in black; (b) 8-noded IEs embedded into the FE mesh.

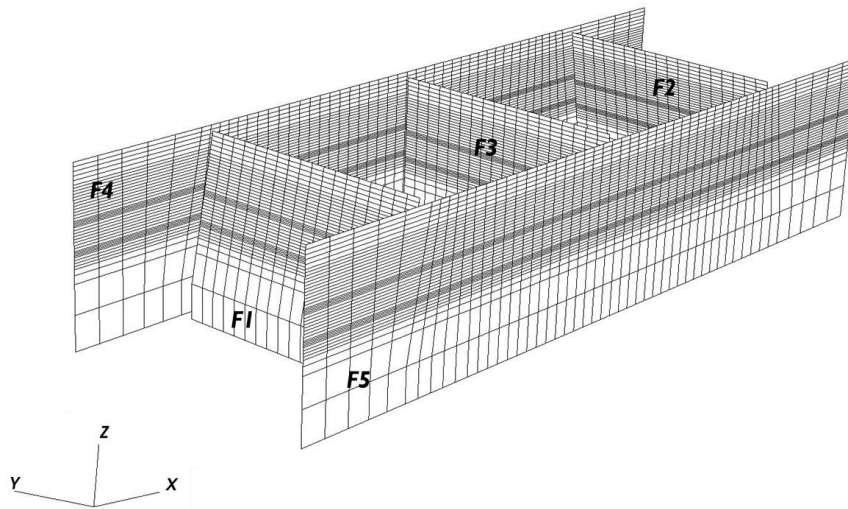


Figure 6: Axonometric view of the IE mesh.

1.4 Reference test case set-up

The reference test case is characterized by the same settings used in KEM-01 [4]:

- The fault F3 is vertical (dip angle equal to 90°).
- The two reservoir blocks have no vertical offset.
- Initial stress field: the direction of the principal stresses corresponds to the x, y, and z axes of the domain, i.e. $\vartheta = 0^\circ$ (Figure 7). The gradient for the vertical stress is layer-dependent, with M1 and M2 (Table I) defined by the ratios $M1 = \sigma_h / \sigma_v$ and $M2 = \sigma_H / \sigma_v$ where σ_h , σ_H and σ_v are the horizontal and vertical principal components of the effective stresses. Figure 8 shows the behaviour of the initial total stresses $\sigma_{TOT,x}$, $\sigma_{TOT,y}$, $\sigma_{TOT,z}$ and the pore pressure P versus depth.
- The Mohr-Coulomb failure criterion governing the fault reactivation is characterized by the cohesion and static friction angle provided in Table I;
- The reservoir formation, overburden, underburden and the Zechstein are linear elastic layers. Only the reservoir formation has a Biot coefficient α not equal to 1. The Young Modulus E and the Poisson coefficient ν are reported in Table I.

- Each fault experiences a pore pressure change ΔP_f that is the average of the pressure change within the two portions of the domain facing the discontinuity.

The above parametrization is summarized in Table I.

Regarding the boundary conditions, zero displacement on the outer and bottom boundaries are prescribed, whereas the land surface is a no-stress boundary.

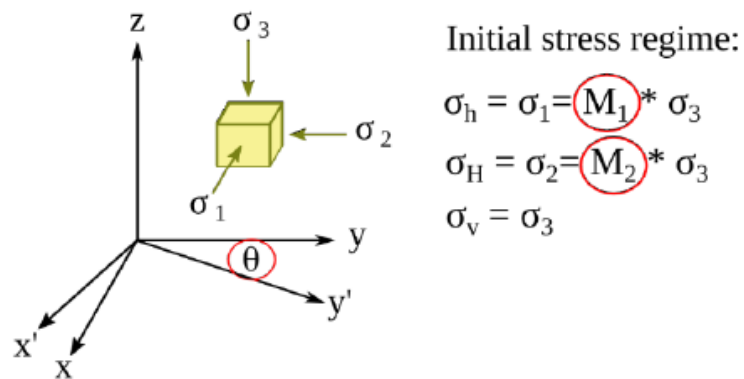


Figure 7: Main parameters used to characterize the fault initial stress.

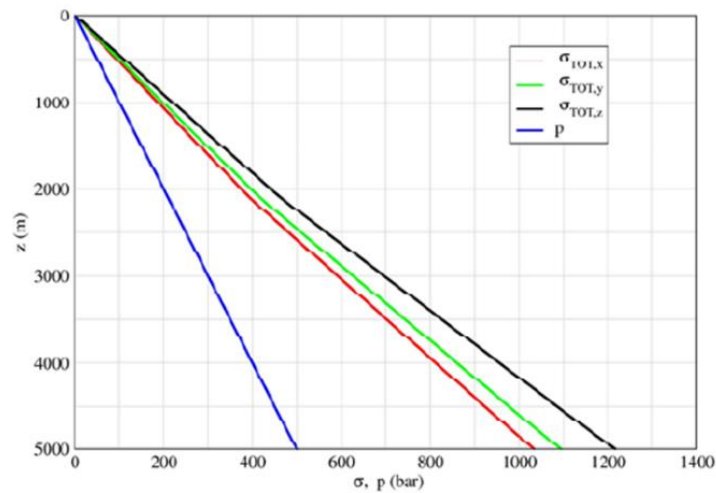


Figure 8: Initial total stress and pore pressure P versus depth used in KEM-01 [3].

PARAMETER	VALUE
F3 dip	90°
Offset	0 m
ϑ	0°
M1	0.74
M2	0.83
cohesion	20 bar
static friction angle	30°
$E_{\text{reservoir}}$	11 GPa
$E_{\text{Zechstein}}$ (below 1800m)	20 GPa
$E_{\text{Zechstein}}$ (from 1800m to 1500m)	35 GPa
$E_{\text{overburden}}$	10 GPa
$E_{\text{underburden}}$	30 GPa
Zechstein	linear elastic
α	0.86
$\nu_{\text{reservoir}}$	0.15
$\nu_{\text{Zechstein}}$	0.30
$\nu_{\text{overburden}}$	0.25
$\nu_{\text{underburden}}$	0.20
ΔP_f	Average between ΔP at the sides of the fault

Table I: Model parameterization for the reference test case.

2 External Forces

The pore pressure change computed in WP3 are used as external forces in to the geomechanical model. As the discretization of the reservoir model is exactly the same used in the geomechanical model, the pore pressure change at the reservoir nodes is simply remapped from the former to the latter (Figure 9-a). According to the KEM-01 model [4], also a pore pressure change within the faults ΔP_f is imposed: that is computed as the average of the pressure change within the two portions of the domain facing the discontinuity (Figure 9-b).

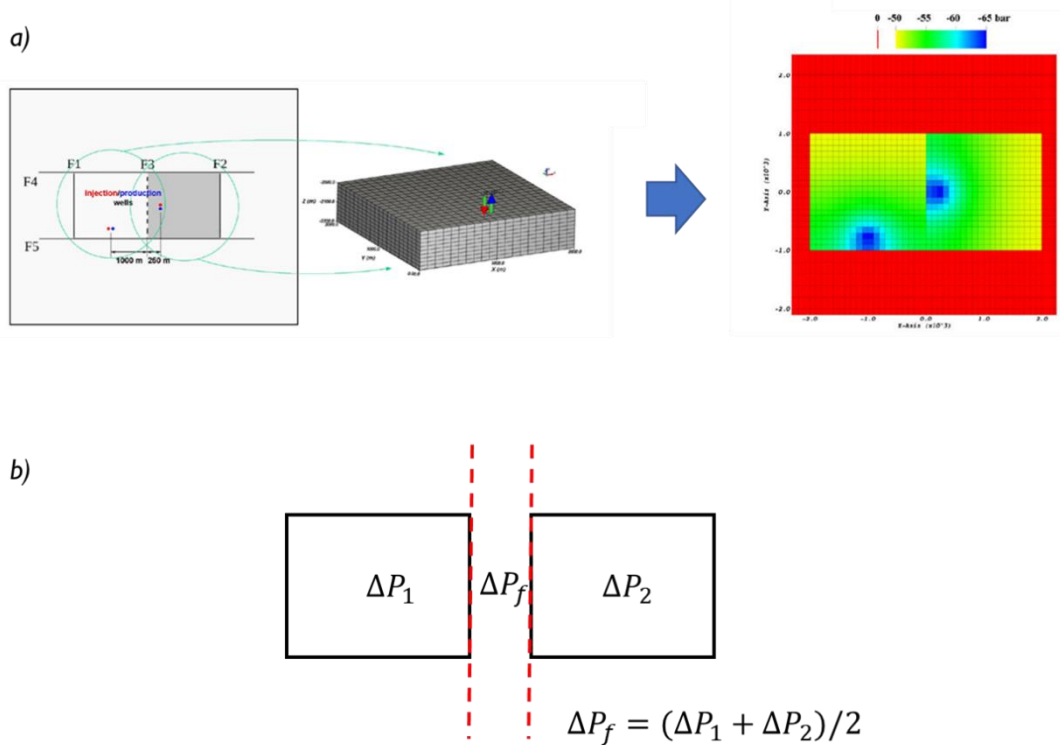


Figure 9: (a) Pressure change remapped from the reservoir model to the geomechanical model; (b) pressure change ΔP_f imposed within the faults.

3 Geochemical Effects

Based on the results obtained in WP1 [6] and WP2 [7], geochemical effects on fault and rock mechanical parameters are evaluated with the goal of implementing them into the geomechanical model. WP1 pointed out that the geochemical effects on the cohesion and friction angle of the faults are negligible while WP2 showed that the laboratory tests on the rocks have ambiguous and contradictory outcomes or even lacking. Regarding the rock exposed to CO₂, both hardening and softening behaviours have been observed. The exposure of rocks to N₂ is expected to have negligible effects while for H₂, there is no quantitative data, but rock degradation is detected.

In agreement with the MEA supervisor, it is decided to:

- neglecting the geochemical effects on fault mechanical parameters;
- for CO₂, evaluate a weakening and a hardening scenario for the reservoir rock, modifying the Young Modulus during the injection phase by -30% and +30%, respectively;
- for N₂, neglecting geochemical effects on the rock mechanical parameters;
- for H₂, evaluate a weakening scenario for the reservoir rock, modifying the Young Modulus during the injection phase by -30%;

4 Numerical Formulation for Fault Modeling

The ATLAS geomechanical software [1] is used for numerical analysis. ATLAS implements an IE formulation according to the Lagrangian approach proposed by Franceschini et al. [5]. With this “element-base” formulation the stress field along the fault surface is computed at the centroid of the 2D element that discretize the faults (Figure 10-a). This approach is preferred to the “node-based” one used in KEM-01 [3], by which the stress field along the fault surface is computed at the nodes (Figure 10-b), because it is numerically more stable, it simplifies the modelling of intersecting faults and it computes a smoothed stress field that facilitates the convergence of the non-linear problem.

On the other hand, since the element-based formulation computes a smoothed stress-field, with the same mesh used in KEM-01 it is not possible to compute the same large stress gradient that arises at the boundaries of the reservoir (Figure 11). To reduce this effect, the mesh is slightly refined at the top and bottom of the reservoir where the 20m-thick elements are subdivided into 10m-thick elements.

This formulation is validated in the next section.

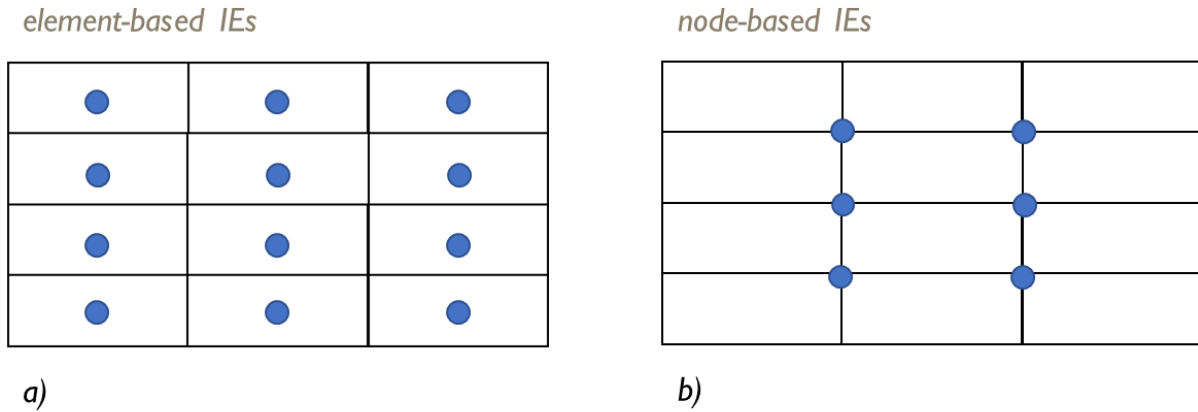


Figure 10: Sketch of the 2D fault discretization, the blue dots highlight where the stress field along the fault surface is computed: (a) at the centroid of the 2D elements for the element-based formulation used in the current project, KEM-39; (b) at the nodes of the 2D elements for the node-based formulation used in KEM-01 project.

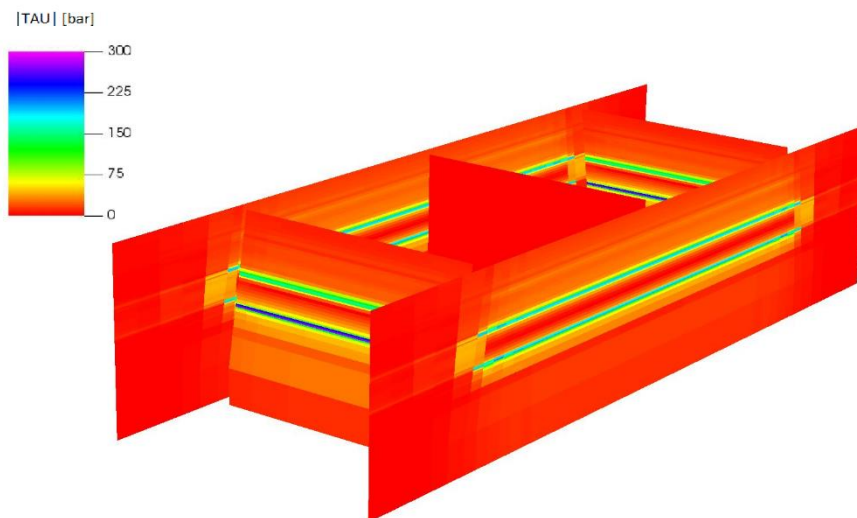


Figure 11: View of shear stress gradients ($\sqrt{\tau_1^2 + \tau_2^2}$) on faults F4 and F5 at the top and bottom of the reservoir for the reference test case at the end of the primary production.

4.1 Validation

The validation is carried out by comparing the solution of the current model (M-39) against that obtained in KEM-01 (M-01) on the following scenarios defined in [4]:

- I a) $E_{Zechstein} = 10 \text{ GPa}$ and no pressure change within the faults, i.e. $\Delta P_f = 0$;
- I b) $E_{Zechstein} = 10 \text{ GPa}$ and the actual pressure change ΔP_f within the faults as defined above;
- I c) $E_{Zechstein} = 20 \text{ GPa} / 35 \text{ GPa}$ and no pressure change within the faults, i.e. $\Delta P_f = 0$;
- I d) $E_{Zechstein} = 20 \text{ GPa} / 35 \text{ GPa}$ and the actual pressure change ΔP_f within the faults. This represents the reference in KEM-01.

For all the scenarios, the pore-pressure change defined in Figure 12 is assigned at the reservoir nodes. The comparison is made in terms of variation in time of the maximum $\chi = |\tau| / \tau_L$ since it is the main outcome of the KEM-01 project. In particular, the maximum χ is computed with a different approach according to the model:

- M-39: χ is computed at the element level and averaged across elements with thickness of 10 m (Figure 13-a);
- M-01: χ is computed at the element level as an average of the values at nodes (Figure 13-a).

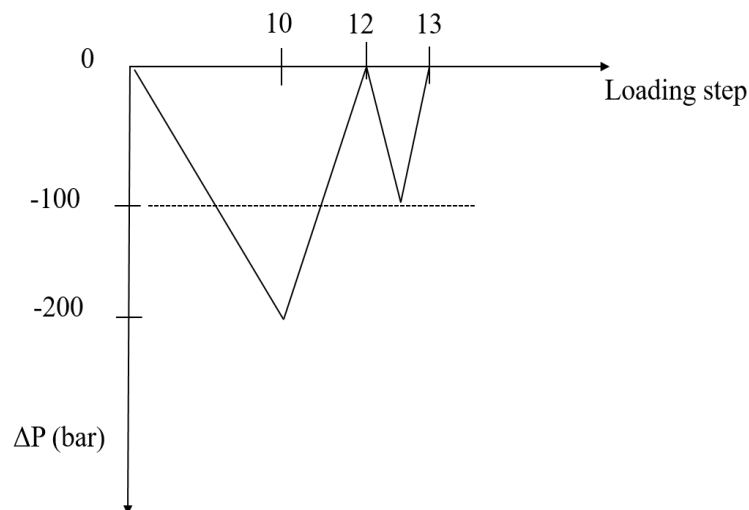


Figure 12: Pore-pressure change assigned at the reservoir nodes in KEM-01 project.

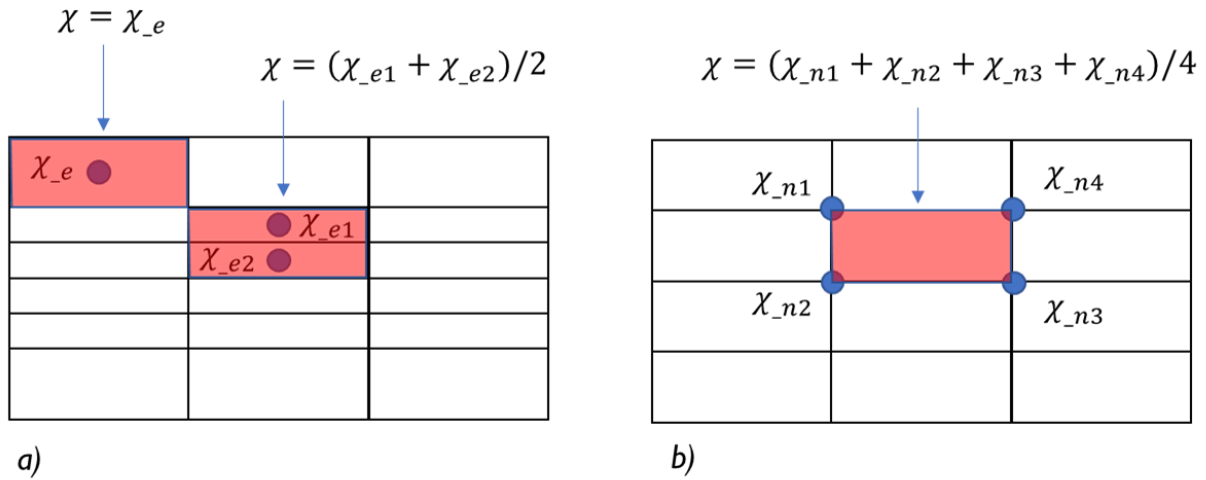


Figure 13: χ computation for: (a) the M-39 model using the element-based formulation; (b) the M-01 model using the node-based formulation.

Figure 14 - Figure 17 show the χ_{\max} distribution at increasing loading step for each fault (F3 is not considered since, for symmetry, it experiences a null shear stress). The small differences are only related to the integral formulation of the finite element method: changing the integration points (mesh and IE formulation) changes locally. The results show that, globally, the two numerical models describe the same physical configuration.

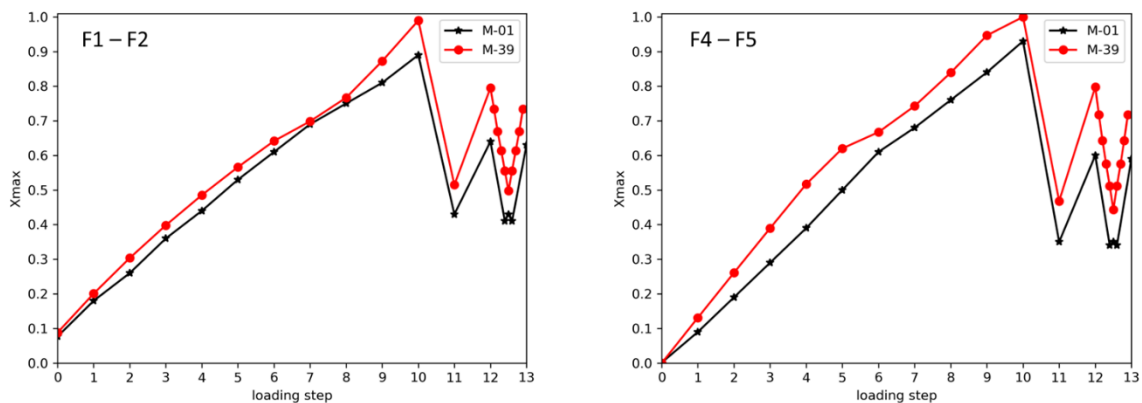


Figure 14: Scenario 1a: χ_{\max} distribution at increasing loading step for each fault. The black line shows the results related to KEM-01 (M-01) while the red line is related to the current model (M-39).

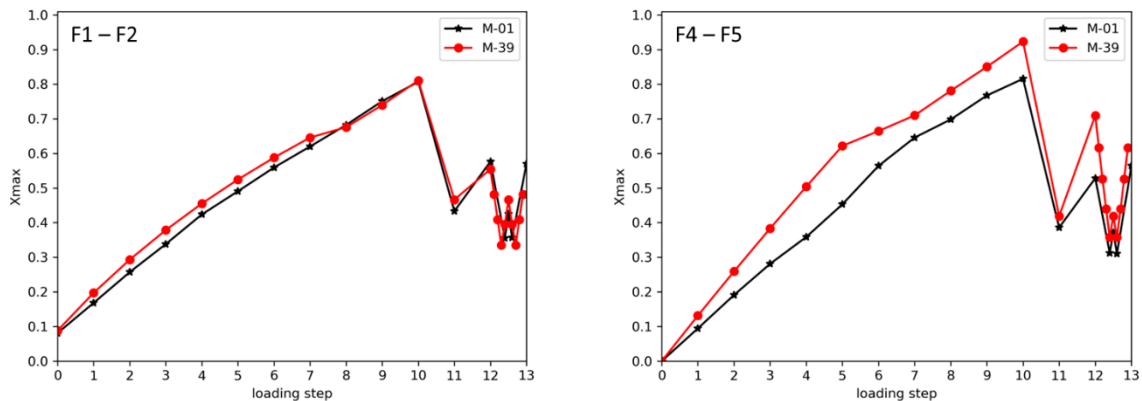


Figure 15: Scenario 1b: χ_{\max} distribution at increasing loading step for each fault. The black line shows the results related to KEM-01 (M-01) while the red line is related to the current model (M-39).

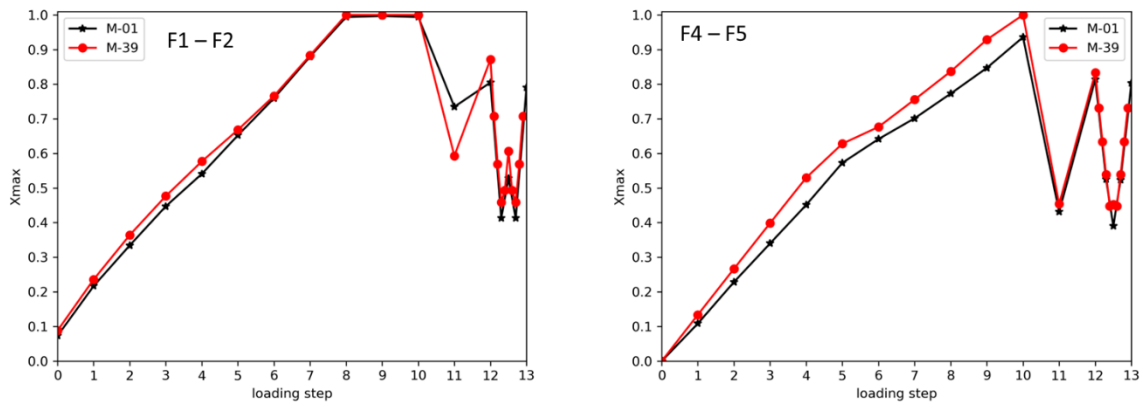


Figure 16: Scenario 1c: χ_{\max} distribution at increasing loading step for each fault. The black line shows the results related to KEM-01 (M-01) while the red line is related to the current model (M-39).

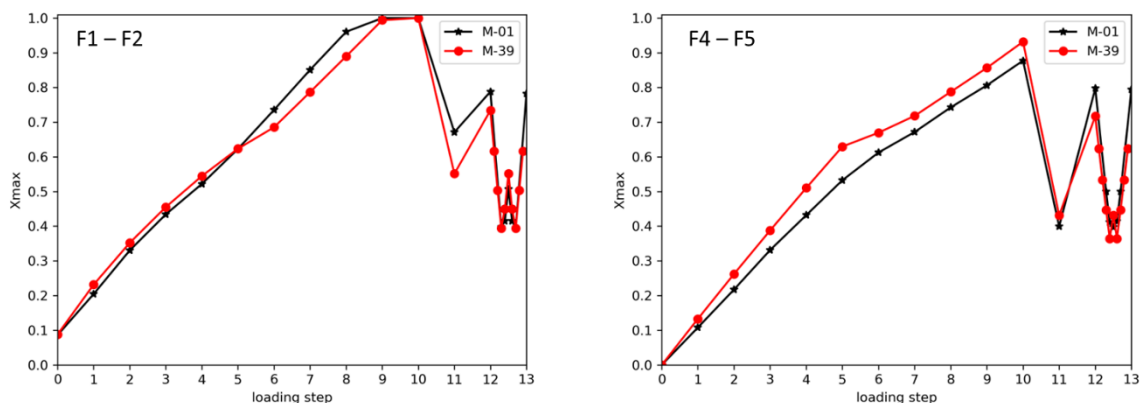


Figure 17: Scenario 1d: χ_{\max} distribution at increasing loading step for each fault. The black line shows the results related to KEM-01 (M-01) while the red line is related to the current model (M-39).

5 Final remarks

Within this WP, the numerical model for the analysis of the CO₂, N₂ and H₂ storage scenarios in KEM-39 project was developed. Compared with the KEM-01 model, it has been updated by introducing geochemical effects depending on the injected fluid. Finally, a validation was performed on different scenarios used in the sensitivity analysis of the KEM-01 project

References

1. ATLAS web page: <https://www.m3eweb.it/atlas>.
2. DICEA, University of Padova. *KEM-01: Safe Operational Bandwidth of Gas Storage Reservoirs – WP2*. Technical Report, 2018.
3. DICEA, University of Padova. *KEM-01: Safe Operational Bandwidth of Gas Storage Reservoirs – WP3*. Technical Report, 2018.
4. DICEA, University of Padova. *KEM-01: Safe Operational Bandwidth of Gas Storage Reservoirs – WP5-6*. Technical Report, 2019.
5. Franceschini, A., Castelletto, N., White, J.A., Tchelepi, H.A. *Algebraically stabilized Lagrange multiplier method for frictional contact mechanics with hydraulically active fractures*. *Computer Methods in Applied Mechanics and Engineering*, Volume 368, 2020, 113161, ISSN 0045-7825, <https://doi.org/10.1016/j.cma.2020.113161>.
6. M3E. *Study within the Mining Effects Knowledge Program (KEM-39) on the cyclic storage of gases in the Netherlands – WP1*. Technical Report, 2022.
7. M3E. *Study within the Mining Effects Knowledge Program (KEM-39) on the cyclic storage of gases in the Netherlands – WP2*. Technical Report, 2022.
8. M3E. *Study within the Mining Effects Knowledge Program (KEM-39) on the cyclic storage of gases in the Netherlands – WP3*. Technical Report, 2022.